A&A 453, 309–319 (2006)
DOI: 10.1051/0004-6361:20054333

Astronomy & Astrophysics

High resolution spectroscopy for Cepheids distance determination

I. Line asymmetry⋆

N. Nardetto[1], D. Mourard[1], P. Kervella[2], Ph. Mathias[1], A. Mérand[2], and D. Bersier[3,4]

[1] Observatoire de la Côte d'Azur, Dept. Gemini, UMR 6203, 06130 Grasse, France
e-mail: Nicolas.Nardetto@obs-azur.fr
[2] Observatoire de Paris-Meudon, LESIA, UMR 8109, 5 place Jules Janssen, 92195 Meudon Cedex, France
[3] Space Telescope Science Institute, 3700 San Martin Drive, Baltimore, MD 21218, USA
[4] Astrophysics Research Institute, Liverpool John Moores University, Twelve Quays House, Egerton Wharf, Birkenhead, CH41 1LD, UK

Received 11 October 2005 / Accepted 11 March 2006

ABSTRACT

Context. The ratio of pulsation to radial velocity (the projection factor) is currently limiting the accuracy of the Baade-Wesselink method, and in particular of its interferometric version recently applied to several nearby Cepheids.
Aims. This work aims at establishing a link between the line asymmetry evolution over the Cepheids' pulsation cycles and their projection factor, with the final objective to improve the accuracy of the Baade-Wesselink method for distance determinations.
Methods. We present HARPS⋆⋆ high spectral resolution observations (R = 120 000) of nine galactic Cepheids: R Tra, S Cru, Y Sgr, β Dor, ζ Gem, Y Oph, RZ Vel, ℓ Car and RS Pup, having a good period sampling (P = 3.39d to P = 41.52d). We fit spectral line profiles by an asymmetric bi-Gaussian to derive radial velocity, Full-Width at Half-Maximum in the line ($FWHM$) and line asymmetry for all stars. We then extract correlations curves between radial velocity and asymmetry. A geometric model providing synthetic spectral lines, including limb-darkening, a constant $FWHM$ (hereafter σ_C) and the rotation velocity is used to interpret these correlations curves.
Results. For all stars, comparison between observations and modelling is satisfactory, and we were able to determine the projected rotation velocities and σ_C for all stars. We also find a correlation between the rotation velocity ($V_{\rm rot} \sin i$) and the period of the star: $V_{\rm rot} \sin i = (-11.5 \pm 0.9) \log(P) + (19.8 \pm 1.0)$ [km s^{-1}]. Moreover, we observe a systematic shift in observational asymmetry curves (noted γ_O), related to the period of the star, which is not explained by our static model: $\gamma_O = (-10.7 \pm 0.1) \log(P) + (9.7 \pm 0.2)$ [in %]. For long-period Cepheids, in which velocity gradients, compression or shock waves seem to be large compared to short- or medium-period Cepheids we observe indeed a greater systematic shift in asymmetry curves.
Conclusions. This new way of studying line asymmetry seems to be very promising for a better understanding of Cepheids atmosphere and to determine, for each star, a dynamic projection factor.

Key words. techniques: spectroscopic – stars: atmospheres – stars: oscillations – stars: variables: Cepheids – stars: distances

1. Introduction

Long-baseline interferometers currently provide a new quasi-geometric way to calibrate the Cepheid Period-Luminosity relation. Indeed, it is now possible to determine the distance of galactic Cepheids up to 1kpc with the Interferometric Baade-Wesselink method, hereafter IBW method (see for e.g. Sasselov & Karovska 1994; and Kervella et al. 2004, hereafter Paper I). Interferometric measurements lead to angular diameter estimations over the whole pulsation period, while the stellar radius variations can be deduced from the integration of the pulsation velocity. The latter is linked to the observational velocity deduced from line profiles by the projection factor p. In this method, angular and linear diameters have to correspond to the same layer in the star to provide a correct estimate of the distance.

The spectral line profile, in particular its asymmetry, is critically affected by the dynamical structure of Cepheids' atmosphere: photospheric pulsation velocity (hereafter $V_{\rm puls}$), velocity gradients, limb-darkening, turbulence and rotation. Thus, radial velocities measured from line profiles, hereafter $V_{\rm rad}$, include the integration in two directions: over the surface, through limb-darkening, and over the radius, through velocity gradients. All these phenomena, except the rotation, are supposed to vary with the pulsation phase. However, they are currently merged in one specific quantity, generally considered as constant with time: the projection factor p, defined as $V_{\rm puls} = pV_{\rm rad}$.

The interferometric definition of the projection factor is of crucial importance in the IBW method, as it can induce a bias of up to 6% on the derived distance (Nardetto et al. 2004; Mérand et al. 2005). Otherwise, the limb-darkening is also required to derive a correct estimation of the angular diameter of the star. With the latest generation of long-baseline interferometers, studying its phase-dependence is of crucial importance (Marengo et al. 2002, 2003; Nardetto et al. 2006).

Line asymmetry was first observed for short-period cepheids by Sasselov et al. (1989). Then, Sasselov et al. (1990) studied

⋆ Tables 3–5 are only available in electronic form at http://www.edpsciences.org

⋆⋆ High Accuracy Radial velocity Planetary Search project developed by the European Southern Observatory.

Table 1. Observed sample of Cepheids sorted by increasing period.

Name	HD	P^a [days]	T_0^a [days]	Nb. of spectra	Nb. of cycles	$m_V{}^b$
R TrA	135592	3.38925	2 451 649.96	14	15	6.66
S Cru	112044	4.68976	2 451 645.64	12	3	6.60
Y Sgr	168608	5.77338	2 451 650.92	17	10	5.74
β Dor	37350	9.84262	2 451 643.54	49	3	3.75
ζ Gem	52973	10.14960	2 451 641.78	50	3	3.90
Y Oph	162714	17.12520	2 451 653.32	7	4	6.17
RZ Vel	73502	20.40020	2 451 633.58	10	3	7.08
ℓ Car	84810	35.551341	2 452 290.4158	118	2	3.74
RS Pup	68860	41.51500	2 451 644.22	15	3	7.03

[a] For ℓ Car, the reference Julian date (T_0) and the pulsation period (P) used to compute the phase are from Szabados (1989). For others stars we used ephemeris from Berdnikov et al. (2001).
[b] The visible magnitude (m_V) is from Berdnikov et al. (2000).

the impact of the asymmetry on radius and distances determinations. The link between line profiles asymmetry and the projection factor has been studied by Albrow et al. (1994). Finally, an error analysis of the IBW method is given in Marengo et al. (2004).

We present here a new original study of the line asymmetry using the very high spectral resolution of HARPS ($R = 120\,000$). We have observed 9 galactic Cepheids with periods ranging from $P = 3.39$ d to $P = 41.52$ d. Radial velocity, full-width at half-maximum (hereafter $FWHM$) and line asymmetry are presented for all stars in Sect. 2.

Section 3 deals with modelling and Sect. 4 with observations interpretation. Through a geometric model different definitions of the projection factor are proposed and compared in order to find the best procedure. Then the model is used to interpret observational radial velocity and asymmetry correlation curves. A set of parameters is thus derived for all stars. Taking into account the whole sample of stars we discuss general properties and in particular the period-dependencies.

2. HARPS observations

2.1. Journal of observations

HARPS is a spectrometer dedicated to the search for extrasolar planets by means of radial velocity measurements. It is installed at the Coudé room of the 3.6 m telescope at La Silla. The resolution is $R = 120\,000$ and the average Signal to Noise Ratio we obtain over all observations in the continuum (292 spectra) is 300 per pixel. The observed sample of Cepheids is presented in Table 1.

We have used the standard ESO/HARPS pipe-line reduction package with a special attention for the normalization process. We have noted on metallic line profiles of all stars a good reproduction from cycle-to-cycle. Therefore, spectra for a given star have been recomposed into an unique cycle.

Using Kurucz models (1992) we have identified about 150 unblended spectral lines. This first study considers only the unblended metallic line Fe I 6056.005 Å.

2.2. A new estimator of the radial velocity, FWHM and asymmetry: the bi-Gaussian

Several methods have been used to measure radial velocities of Cepheids, each having advantages and drawbacks. Among these methods there is the line minimum (usually determined via a parabolic fit to a few pixels near the bottom of the line) a Gaussian fit (obviously not adequate for asymmetric lines), the line centroid, determined from the integration of the line profile (requires high *Signal*/*Noise* ratio), and the line bisector where one measures the width of the line at one or several depths. Our bi-Gaussian approach combines advantages of methods useful for low S/N data while providing information usually associated with high resolution and high S/N data (asymmetry).

Radial velocity, full width at half-maximum ($FWHM$) and asymmetry have been derived simultaneously applying a classical χ^2 minimization algorithm between the observed line profile ($S(\lambda)$) and a modelled spectral line profile ($f(\lambda)$). The corresponding reduced χ^2 is:

$$\chi_{\rm red}{}^2 = \frac{1}{N-\nu}\sum_{i=0}^{N}\frac{(S(\lambda_i)-f(\lambda_i))^2}{\sigma(\lambda_i)^2} \quad (1)$$

with N the number of pixel in the spectral line, ν the number of degrees of freedom and $\sigma(\lambda_i) = SNR * f(\lambda_i)$ is the statistical uncertainty associated to each pixel. SNR is the estimate of the Signal to Noise Ratio in the continuum.

The analytic line profile is defined by:

$$f(\lambda) = 1 - D\exp\left(\frac{4\ln 2(\lambda-\lambda_{\rm m})^2}{(FWHM(1+A))^2}\right) \text{ if } \lambda > \lambda_{\rm m} \quad (2)$$

and

$$f(\lambda) = 1 - D\exp\left(\frac{4\ln 2(\lambda-\lambda_{\rm m})^2}{(FWHM(1-A))^2}\right) \text{ if } \lambda < \lambda_{\rm m} \quad (3)$$

with four free parameters:

- D, the depth of the line. This quantity has no dimension;
- $\lambda_{\rm m}$, the wavelength associated to the minimum of the line (in Å). The corresponding radial velocity is noted $RV_{\rm m}$;
- $FWHM$ is the Full-Width at Half-Maximum in the line, also in Å;
- A is the asymmetry as a percentage of the $FWHM$.

The $4\ln 2$ factor is to obtain a correct definition of the $FWHM$. Forcing asymmetry to zero in this minimization process is equivalent to fitting a Gaussian to the line profile. In this case we can derive another type of radial velocity noted $RV_{\rm g}$.

There are different ways to define the line asymmetry (see e.g. Sasselov et al. 1990; Sabbey et al. 1995). The advantage of the bi-Gaussian method is that it offers the possibility to derive statistical uncertainties directly from the minimization process.

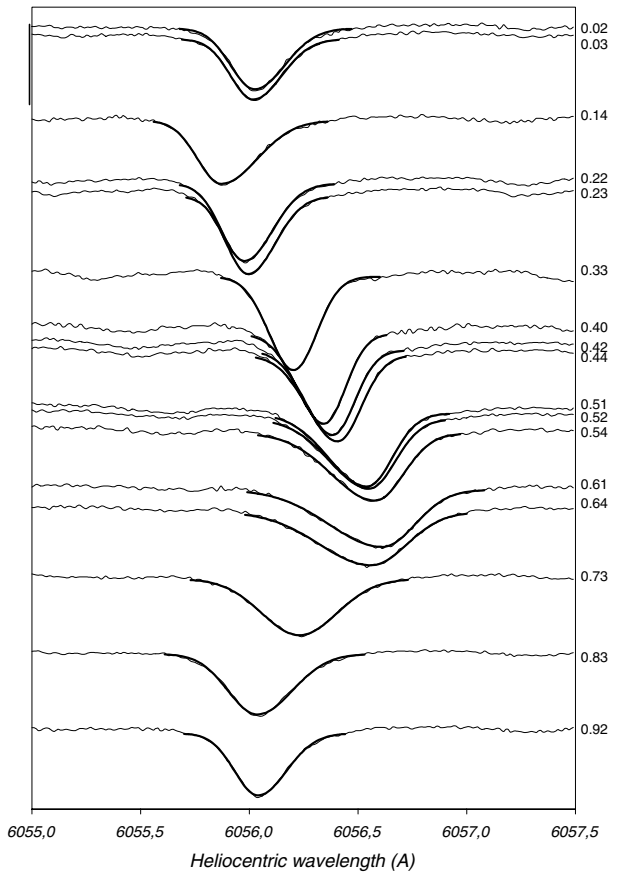

Fig. 1. Spectral line evolution of β Dor together with the modelled bi-Gaussian (bold). Line asymmetry is clear. The vertical line at the top corresponds to a differential flux of 0.3. Pulsation phases are given on the right of each profile.

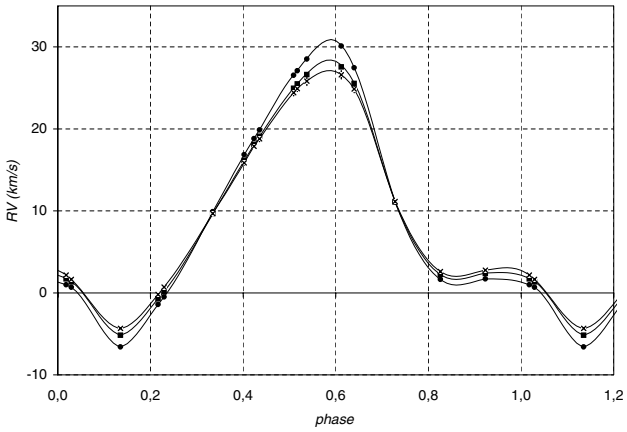

Fig. 2. β Dor radial velocities obtained with different method: $RV_{\rm m}$ (points), $RV_{\rm g}$ (squares), and $RV_{\rm c}$ (crosses). Statistical uncertainties at $\pm 1\sigma$ are indicated but too small to be visualized. We can therefore see the impact of the choice of the method in the case of a very asymmetric line (Fig. 1).

Moreover, all parameters ($RV_{\rm m}$, $FWHM$, D and A) are fitted simultaneously leading to a very consistent set of information. The largest reduced χ^2 we obtain with this method is of about 10 corresponding to a SNR of 438, but in most cases we have a reduced $\chi^2 \simeq 1$ or 2 corresponding to a SNR ranging from 75 to 350. That means that our analytic model is well suited to the data quality. We note also that the reduced χ^2 is not sensitive to the spectral line resolution.

As an example, Fig. 1 presents line profile variation for β Dor together with the analytic spectral line profile. We find that the asymmetry is insensitive to the choice of the continuum. However, this one has to be correctly defined to derive correct values of the $FWHM$ and line depth D.

Another radial velocity definition, the centroid velocity ($RV_{\rm c}$) or, the first moment of the spectral line profile, has been estimated as:

$$RV_{\rm c} = \frac{\int_{\rm line} \lambda S(\lambda) {\rm d}\lambda}{\int_{\rm line} S(\lambda) {\rm d}\lambda}. \quad (4)$$

Tables 3−5 present the resulting values of $RV_{\rm g}$, $RV_{\rm m}$, $RV_{\rm c}$, $FWHM$, D, A, SNR and $\chi^2_{\rm red}$ together with the corresponding uncertainties computed from the fitting method.

2.3. Radial velocity

As indicated in the previous section, we can derive three types of radial velocity: the velocity associated to the Gaussian fit ($RV_{\rm g}$), the line minimum ($RV_{\rm m}$) and the barycenter of the spectral line ($RV_{\rm c}$). Figure 2 shows these radial velocity curves obtained in the case of β Dor. Figure 3 represents for each star of our sample, the $RV_{\rm m}$ variation (arbitrary shifted). The solid lines are the interpolated curves using a periodic cubic spline function. This function is calculated either directly on the observational points (e.g. β Dor) or using arbitrary pivot points (e.g. RZ Vel). In the latter case, a classical minimization process between observations and the interpolated curve is used to optimize the position of the pivot points. All the interpolated curves presented in this study are derived using one of these two methods. The only exception is Y Oph (too few points) for which we performed a linear interpolation.

2.4. The Full-Width at Half-Maximum in the line

Figure 4 presents the $FWHM$ curve as a function of phase for all stars. We note that the largest $FWHM$ values are obtained for the maximum contraction velocities. RS Pup, the longest period Cepheid of our sample, seems to present an important compression or shock wave signature. Figure 5 presents line profile variation for this star. Unfortunately the phase coverage is not very good, but we can clearly see a strong increase of the $FWHM$ at $\phi = 0.83$. Such phenomenon has been already detected in β Cepheids (Fokin et al. 2004).

2.5. Asymmetry

Figure 6 shows the asymmetry variation for all stars. Generally speaking, the shape of the aymmetry curve is similar to the shape of the velocity curve $RV_{\rm m}$.

As already mentioned in Sect. 2.3, the radial velocity according to the choice of the method considered is sensitive to the line asymmetry. Figure 7 shows the correlation between the differences of radial velocity ($\Delta V = RV_{\rm m} - RV_{\rm g}$) and the asymmetry of the line. We have only presented here the case of ℓ Car and RS Pup. Each star presents a similar behavior. A typical difference in velocity of about 4 km s^{-1} can be obtained for an asymmetry of 40% in extreme cases (Y Sgr and R TrA). The relation between the radial velocity difference and the asymmetry is certainly affected by star characteristics (rotation, $FWHM$, velocity gradients) present in the line asymmetry. In particular

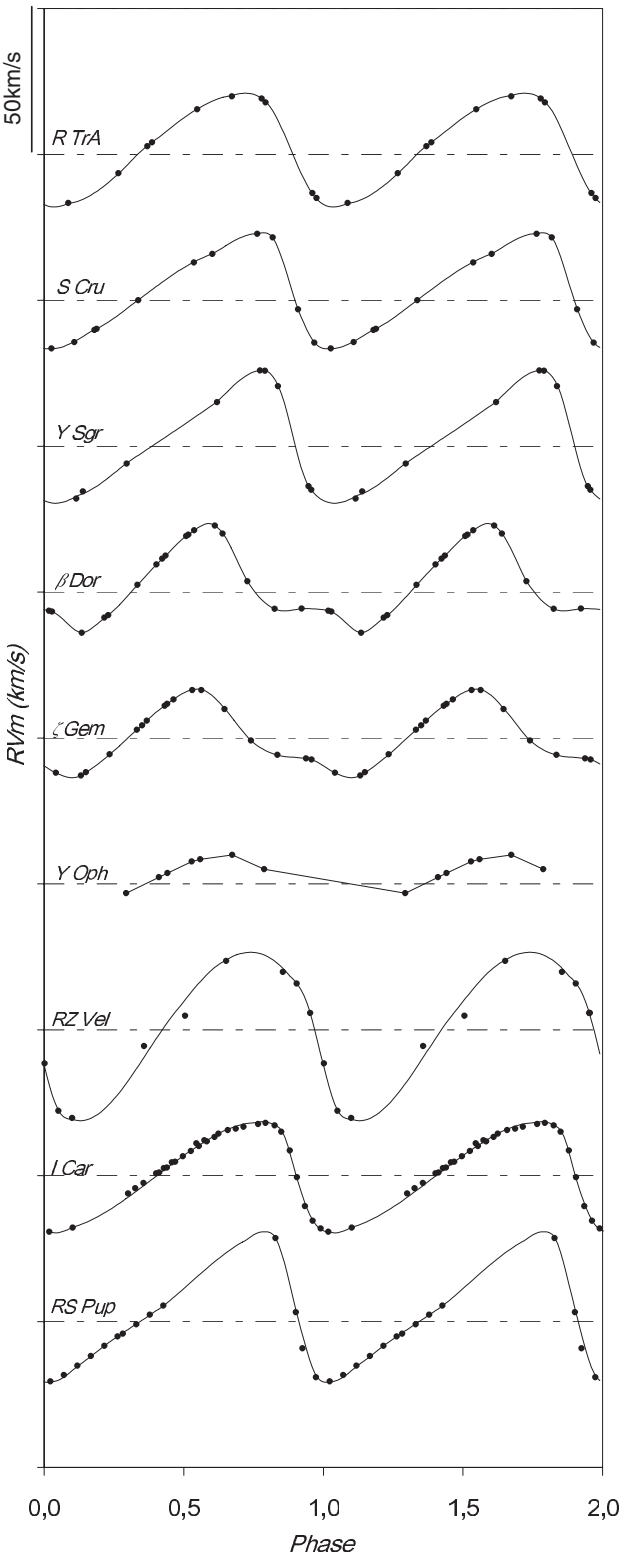

Fig. 3. Radial velocity curves ($RV_{\rm m}$). Curves have been arbitrarily shifted vertically. The horizontal lines are the zero velocity in the stellar rest frame. Largest velocities are for receding motion.

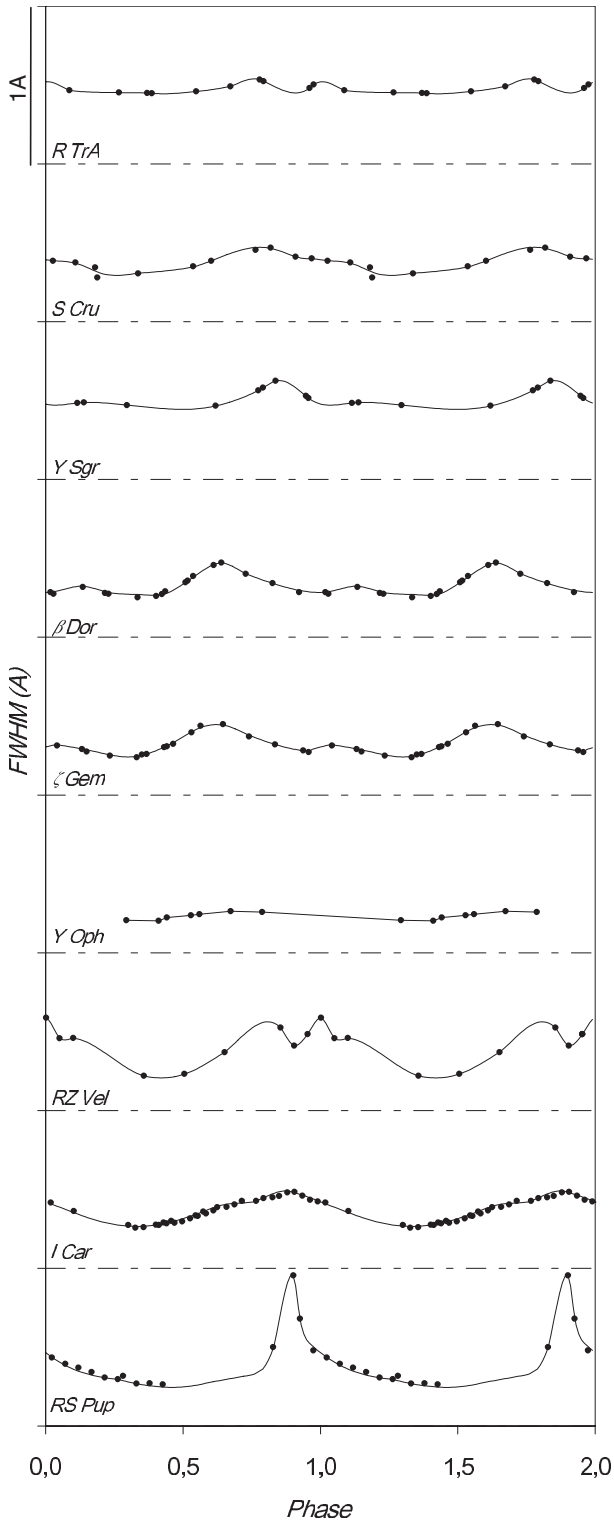

Fig. 4. *FWHM* versus phase for all stars. Curves have been arbitrarily shifted vertically. The horizontal lines correspond to a zero *FWHM*. Note the particular case of RS Pup, which may present the signature of an important compression or shock wave. RS Pup has the longest period of our sample.

RS Pup signature is certainly affected by strong velocity gradient effects. The fact that the $RV_{\rm m}$ and $RV_{\rm g}$ radial velocities present such differences as a function of the pulsation phase is an additional difficulty concerning an average projection factor and its time-dependence determination. With the centroid estimator of the radial velocity ($RV_{\rm g} - RV_{\rm c}$ or $RV_{\rm m} - RV_{\rm c}$) results are quite similar.

In next sections, we summarize all observational results in correlation diagrams between radial velocity and asymmetry. These correlations are interpreted using the geometric model

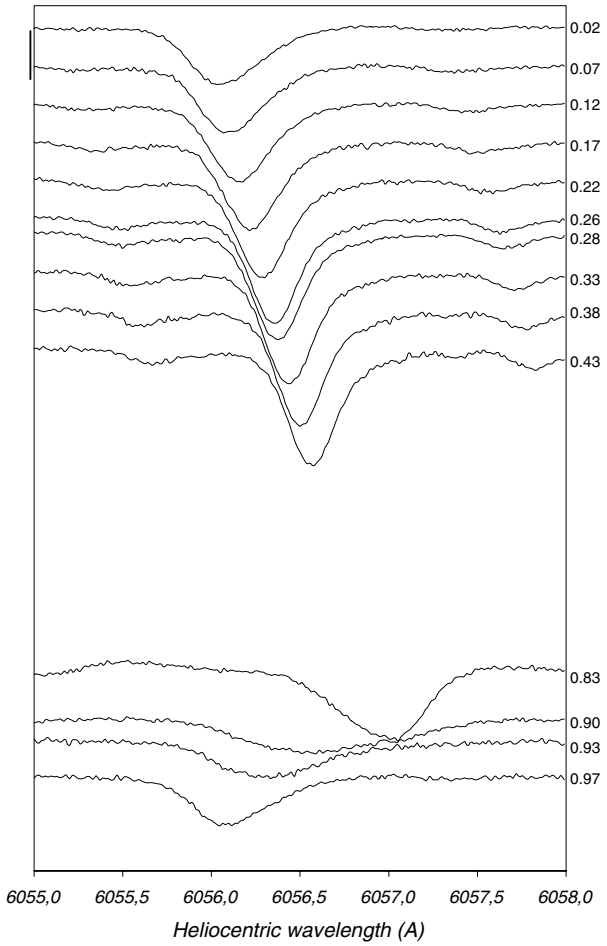

Fig. 5. FeI 6056.005 Å spectral line evolution of RS Pup. The vertical line at the top corresponds to a differential flux of 0.2. We note the broadening of the line at $\phi = 0.83$ which could be the signature of a strong velocity gradient (compression or shock wave).

in order to determine some physical parameters of our stars and to obtain information about dynamical effects in Cepheids atmosphere.

3. A toy model

We consider a limb-darkened pulsating star in rotation with an one-layer atmosphere. Our model has four parameters:

- the limb-darkening of the star: we consider a linear law for the continuum-intensity profile of the star defined by $I(\cos(\theta)) = 1 - u_V + u_V \cos(\theta)$, where u_V is the limb-darkening of the star in V band (Claret et al. 2000). Its value is about 0.7 for Cepheids. θ is the angle between the normal of the star and the line-of-sight;
- the projected rotation velocity $V_{\rm rot} \sin i$, where i is the angle between the line-of-sight and the rotation axis (in km s^{-1});
- the pulsation velocity (in km s^{-1});
- the width of the spectral line (in Å), hereafter named $\sigma_{\rm C}$. It is the $FWHM$ of the line with no pulsation nor rotation velocities. It is supposed to be constant with the pulsation phase.

The velocity field is a combination of pulsation and rotation velocities. Through the Doppler effect, this field can be transposed into wavelengths, and weighted by the surface brightness (limb-darkening) to obtain the weighting of the spectral line. We have

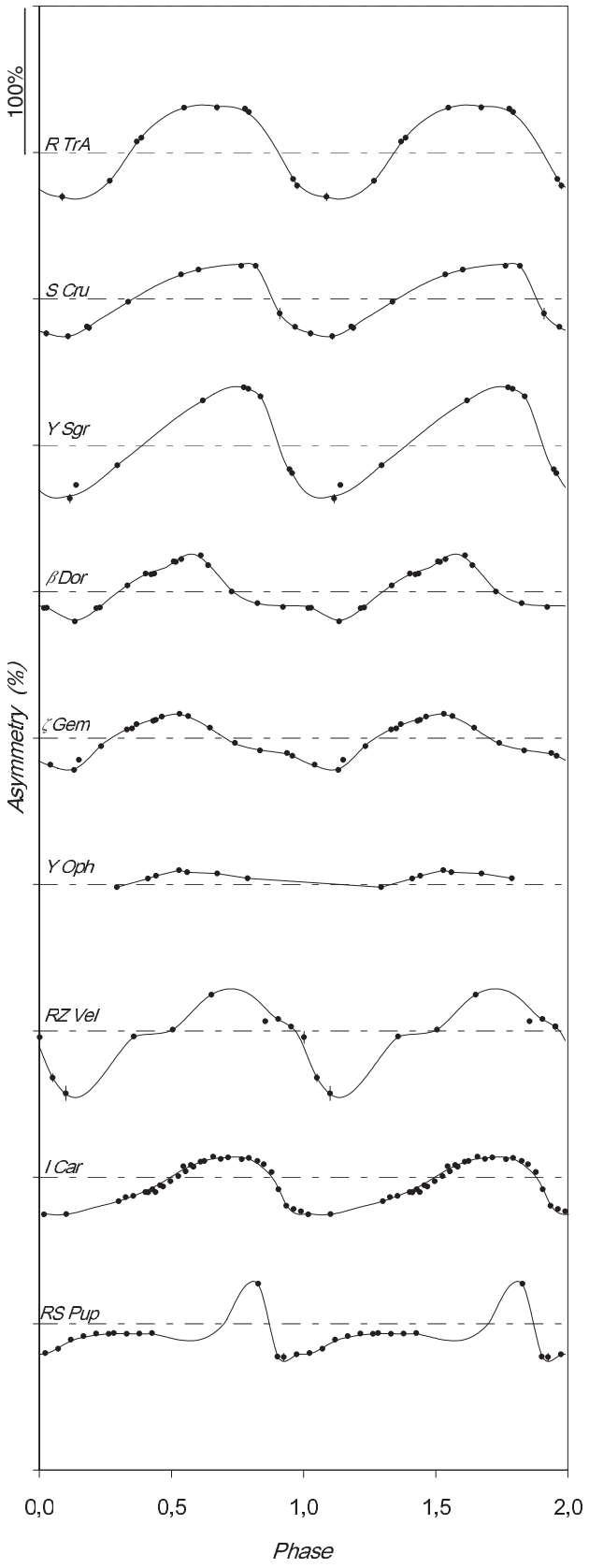

Fig. 6. Asymmetry against phase for all stars. Curves have been arbitrarily shifted vertically. The horizontal lines correspond to an asymmetry of zero.

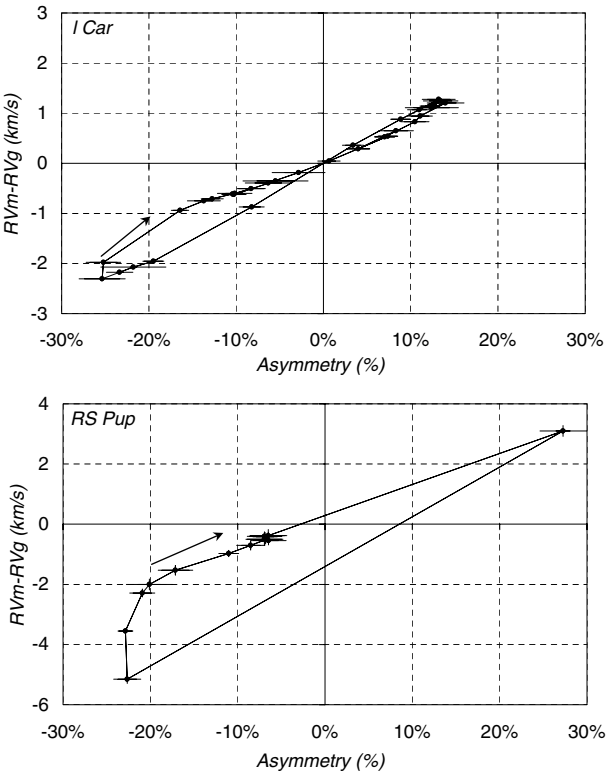

Fig. 7. Difference between the radial velocity obtained with the line minimum and the Gaussian fit methods as a function of the asymmetry in the case of ℓ Car and RS Pup. Statistical uncertainties are provided for each point. Arrows indicate the direction and the origin $\phi = 0$ of the curves. These relations are not linear and certainly affected by star characteristics (rotation, *FWHM*, velocity gradients...).

then to convolve it with the intrinsic profile to obtain the synthetic spectral line profile. The weighting or the synthetic spectral line profile are presented in different cases in Fig. 8.

We now consider a pulsation velocity curve defined by:

$$V_{\rm puls}(\phi_i) = V_{\rm max} \cos(2\pi\phi_i) \quad (5)$$

with a typical value for the maximal pulsation velocity of $V_{\rm max} = 30\ {\rm km\,s^{-1}}$. This relation which is a poor approximation of the pulsation velocity curve is only used for the projection factors determination (see below). It has no incidence on the results (see Sect. 4.1). From the synthetic spectral line profiles, we perform a bi-Gaussian fit to derive the four parameters described in Sect. 2.2: D, $\lambda_{\rm m}$, *FWHM* and A. Then we derive the $RV_{\rm m}$, $RV_{\rm g}$, $RV_{\rm c}$ velocities, and the corresponding radial velocity-asymmetry correlation curves (hereafter RV-A plot). In Fig. 10, the RV-A plots are represented for different values of the $\sigma_{\rm C}$ and rotation parameters. The limb-darkening (considered as constant with the pulsation phase) has a very small effect in the weighting of the line profile and thus practically no impact on the RV-A plot. Applying a classical minimization process between the pulsation and radial velocities, we have also derived for each set of parameters the corresponding constant projection factors: $p_{\rm m} = \frac{V_{\rm puls}}{RV_{\rm m}}$, $p_{\rm g} = \frac{V_{\rm puls}}{RV_{\rm g}}$ and $p_{\rm c} = \frac{V_{\rm puls}}{RV_{\rm c}}$.

Firstly, we note that the $\sigma_{\rm C}$ of the line and the rotation have different effects on the slope and/or shape of the correlation curves.

Secondly, correlation curves are slightly different from one definition of radial velocity to another. But the interesting point is that the $RV_{\rm c}$ velocity does not depend of $\sigma_{\rm C}$ and/or rotation.

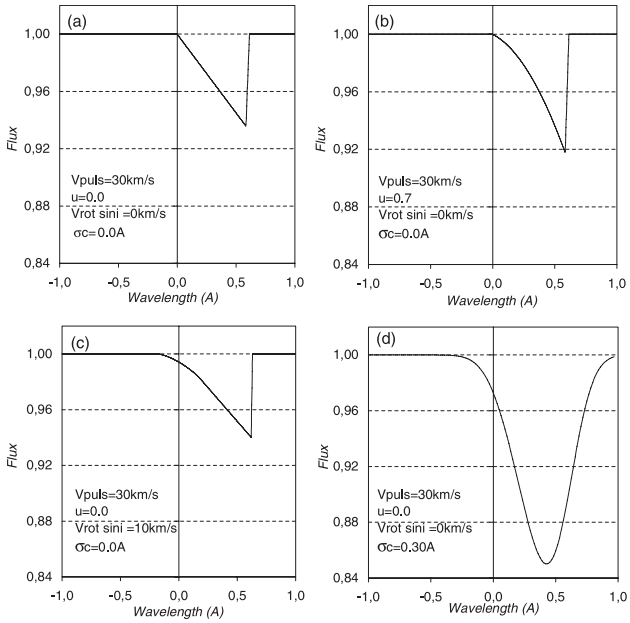

Fig. 8. The weighting or the synthetic spectral line profile in different cases, considering **a)** the pulsation velocity, **b)** the limb-darkening, **c)** the rotation and, **d)** an intrinsic width for the line ($\sigma_{\rm C}$).

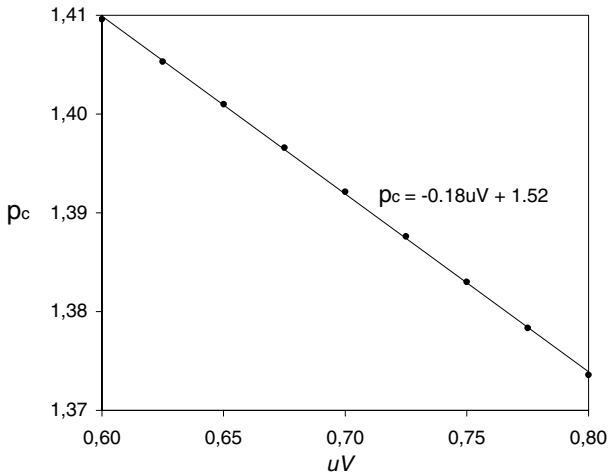

Fig. 9. The projection factor corresponding to the centroid velocity ($p_{\rm c}$) as a function of the limb-darkening parameter (u_V). Dots are the results from the toy model and the solid line corresponds to the linear approximation ($\chi^2 \simeq 10^{-5}$).

This behavior is clearly seen on diagrams 10b and 10d: the centroid projection factor $p_{\rm c}$ is constant with the $\sigma_{\rm C}$ and the rotation while the Gaussian and the minimum projection factors, $p_{\rm g}$ and $p_{\rm m}$, are varying. For the Cepheids of our sample the centroid projection factor ranges from $p_{\rm c} = 1.40$ ($u_V = 0.64$; R TrA) to $p_{\rm c} = 1.38$ ($u_V = 0.75$; ℓ Car), through the following relation:

$$p_{\rm c} = -0.18 u_V + 1.52 \quad (6)$$

This relation is a linear approximation from the geometrical model (see Fig. 9). Note that the geometrical model does not contain the physics of the pulsations, and thus the relation may not hold when instead of u_V a more realistic limb-darkening (taking into account hydrodynamic effects) is used. In particular, hydrodynamic effects can result in a much larger limb-darkening, especially at the wavelengths corresponding to spectral line (see e.g. Marengo et al. 2003).

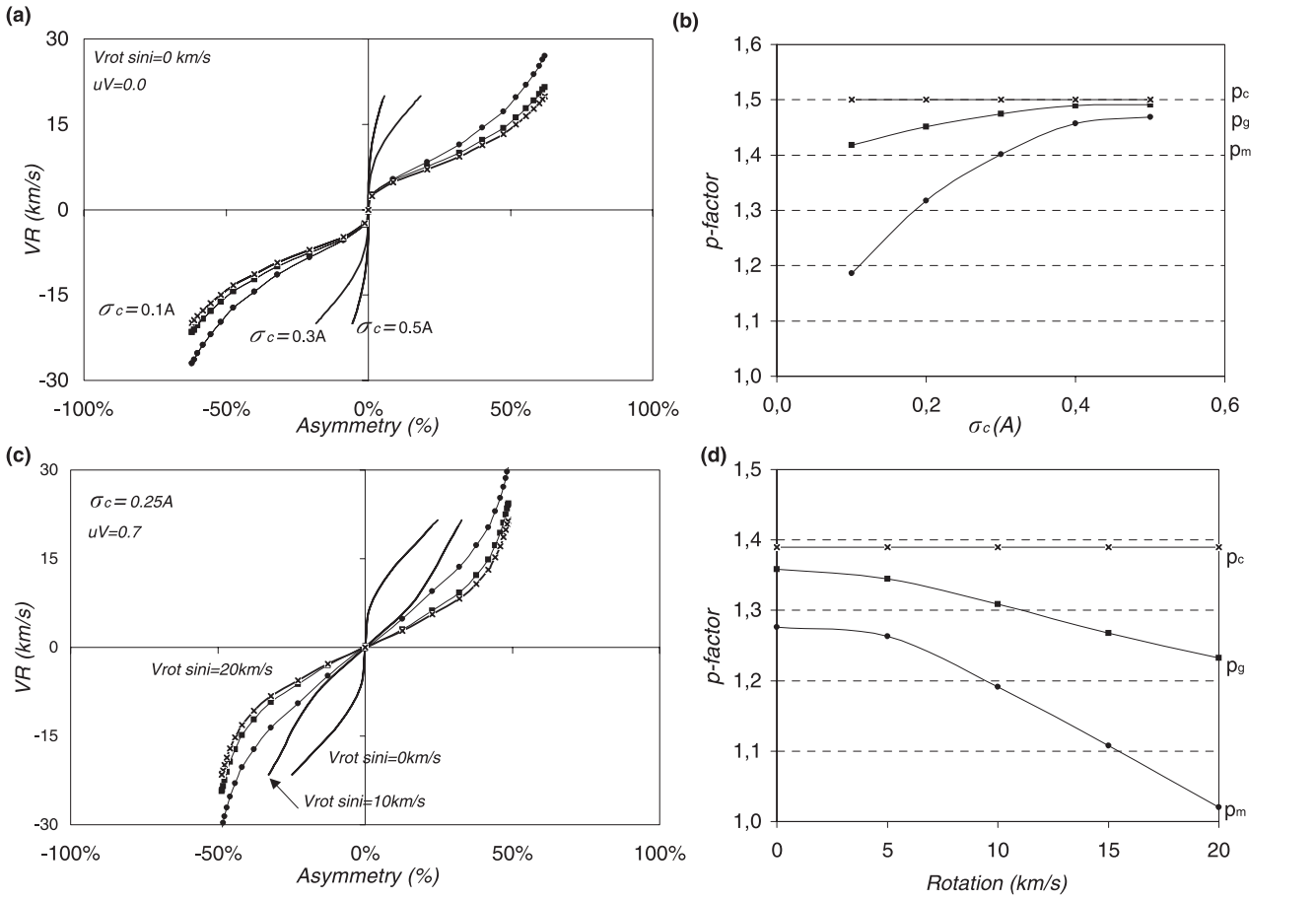

Fig. 10. Results of the geometric model of pulsating star. **a)**, **b)** The radial velocity-asymmetry correlation curves for different σ_C, with no rotation and no limb-darkening (uniform disk). Points, squares and crosses correspond respectively to the RV_m, RV_g and RV_c radial velocities. For clarity RV_g and RV_m are represented only for $\sigma_C = 0.1$ Å. The solid lines are the interpolated curves using a cubic spline function. The corresponding projection factors are represented on diagram **b)**. **c)**, **d)** Same plots but for different values of the rotation. The σ_C and the limb-darkening are respectively of 0.25 Å and 0.7. These RV-A plot are used to interpret HARPS observations.

This behavior is of great importance in the context of the IBW method. Indeed, the community has often used the p_c = 1.36 value of the projection factor (Burki et al. 1982) using the Gaussian method instead of the centroid method. As seen here, and already pointed out by Burki et al. (1982), this estimator is biased by the rotation velocity, even if Cepheids are supposed to be slow rotators, and also by the σ_C. We thus recommend the centroid based methods (spectral observable and p-factor) for the analysis of Cepheid radial velocities. For the present work, we have therefore chosen the RV_c definition of the radial velocity. Even though this requires substantial S/N, its advantages outweigh the drawback of spending more telescope time to acquire the data.

4. Interpretation

4.1. Methodology

Modeling results obtained in the previous section are now helpful to elaborate a strategy in a comparison of observations and models.

Firstly, the effective temperature $T_{\rm eff}$ and the surface gravity $\log g$ have been used to derive the intensity profile of stars through linear limb-darkening coefficients u_V of Claret et al. (2000) (see Table 2).

Secondly, we determine the projection factor p_c using Eq. (6). The pulsation velocity is then derived through $V_{\rm puls} = p_c RV_c$, where RV_c is the observational radial velocity corrected from the heliocentric velocity given in Table 2. The pulsation velocity $V_{\rm puls}$ and the projection factor p_c (see Table 2) obtained are not physically realistic, because our model does not include dynamical effects and in particular velocity gradients in the atmosphere, nevertheless this procedure imposes the surimposition of observational and modelled radial velocity curves RV_c. Moreover, as a very good agreement is observed for each phase (better than 1%), it validates the use of a *constant* projection factor (p_c). We find also that the poor description of the pulsation velocity (Eq. (5)) used to derive p_c has no incidence on the resulting modelled RV_c curve. By this procedure, we can thus concentrate only on the asymmetry, making the interpretation easier. Note that Nardetto et al. (2004) already gave an indication of the impact of velocity gradients on the projection factor, and thus on the distance determination, in the case of δ Cep (about −6%). In Table 2, we also indicate for each star the corresponding projection factors p_g and p_m for comparison.

Thirdly, σ_C and $V_{\rm rot} \sin i$ are determined together from the observational RV-A and $FWHM$ curves. We first consider the minimum of the observational $FWHM$ curve to obtain an indication on the value of σ_C. We then find the rotation which gives the best slope and shape for the RV-A curve. But as the rotation has also an impact on the $FWHM$ (about 0.02 Å), we have then

Table 2. Optimized parameters obtained for each sample Cepheid through the confrontation of HARPS observations with our geometric model.

stars	R TrA	S Cru	Y Sgr	β Dor	ζ Gem	Y Oph	RZ Vel	l Car	RS Pup
Period	3.38925	4.68976	5.77338	9.84262	10.14960	17.12520	20.40020	35.551341	41.51500
mean $T_{\rm eff}$[a][K]	6354	5995	5350	5490	5727	5907	5537	5091	5143
mean $\log(g)$[a]	2.0	1.9	1.0	1.8	1.5	1.5	1.5	1.5	0.4
u_V^b	0.6371	0.6541	0.7194	0.6999	0.6721	0.6514	0.6970	0.7541	0.7121
$v_\gamma{}^c$ [km s^{-1}]	−13.2	−7.1	−2.5	7.4	6.9	−6.6	24.1	3.6	22.1
$\sigma_{\rm C}^d$ [Å]	0.29	0.27	0.27	0.23	0.23	0.20	0.23	0.25	0.30
$V_{\rm rot}\sin i^e$ [km s^{-1}]	15	10	16	6	6	4	3	7	<1
$p_{\rm m} = \frac{V_{\rm puls}}{RV_{\rm m}}$	1.13	1.23	1.10	1.23	1.23	1.23	1.26	1.23	1.31
$p_{\rm g} = \frac{V_{\rm puls}}{RV_{\rm g}}$	1.28	1.31	1.26	1.32	1.32	1.33	1.34	1.31	1.36
$p_{\rm c} = \frac{V_{\rm puls}}{RV_{\rm c}}$	1.40	1.40	1.39	1.39	1.40	1.40	1.39	1.38	1.39
$\gamma_{\rm O}^e$ [%]	3.3	0.7	2.0	0.2	−2.4	–	−3.2	−6.9	−6.5
$\gamma_{\rm C}^g$ [%]	3.1	4.3	0.4	2.9	0.5	–	1.4	1.2	0.6
$\gamma_{\rm O-C}^h$ [%]	0.2	−3.6	1.6	−2.7	−2.9	–	−4.6	−8.2	−7.1

[a] $T_{\rm eff}$[K] and $\log(g)$, deduced from Gieren et al. (1998) for R TrA, S Scu, Y Oph and RZ Vel. For Y Sgr, β Dor, ζ Gem, ℓ Car, and RS Pup these quantities have taken from Cayrel de Strobel et al. (1997, 2001).
[b] u_V from Claret et al. (2000).
[c] v_γ from Galactic Cepheid database (online: `http://www.astro.utoronto.ca/DDO/research/cepheids`).
[d] Uncertainty on $\sigma_{\rm C}$ is of about 0.02 Å.
[e] Uncertainty on $V_{\rm rot}\sin i$ is of about 1 km s^{-1}.
[f] $\gamma_{\rm O}$ [%] is the averaged value of the observational asymmetry curves. The associated statistical uncertainties are of the order of 0.3%.
[g] $\gamma_{\rm C}$ [%] is the averaged value of the computed asymmetry curves.
[h] $\gamma_{\rm O-C}$ [%] is the average value of the O−C asymmetry curve.

to slightly readjust $\sigma_{\rm C}$ accordingly. By this process we finally find the best and unique values for $\sigma_{\rm C}$ and $V_{\rm rot}\sin i$.

The uncertainties on $V_{\rm rot}\sin i$ and $\sigma_{\rm C}$, associated to the minimization process, were estimated to be respectively 1 km s^{-1} and 0.02 Å. Similar uncertainties are found if one considers several metallic lines. Note however that our toy model is too simple to provide secure and precise values of the rotation, which is the most interesting parameter. In particular the broadening of the spectral line due to the macro-turbulence can certainly affect our rotation values (Bersier & Burki 1996). Nevertheless our principal and first objective is to probe the dynamical effects by a direct comparison of our static model with observations.

4.2. Observations versus modelisation

We now apply our methodology to each Cepheid of our sample. Results are indicated in Table 2. RV-A plot are represented in Figs. 11 and 12. Note that RV-A plot deduced from the model have been shifted in asymmetry to match the observations (this point is discussed in next section). For R TrA and Y Sgr, we can notice a very small slope for the RV-A plot and a very large value for the observational $FWHM$. It indicates a large rotational velocity $V_{\rm rot}\sin i$ and a properly small value for $\sigma_{\rm C}$ (see Figs. 10a,c). Thus, the corresponding Gaussian and minimum projection factors ($p_{\rm g}$ and $p_{\rm m}$) are lower than for others stars (see Figs. 10b,d). Conversely, for Y Oph and RZ Vel the RV-A plot have relatively large slope while the observational $FWHM$ is typical (about 0.3). This has a direct consequence on the rotation, which is then very small, and on the projection factors ($p_{\rm g}$ and $p_{\rm m}$) which are then relatively large. Comparatively, S Cru, β Dor and ζ Gem can be considered as intermediate cases. For ℓ Car and RS Pup, we obtain an atypical RV-A plot which is greatly shifted in asymmetry. For RS Pup, we obtain a specific RV-A plot characterized by a strong curvature which can be interpreted by our geometric model as a very slow rotation velocity $V_{\rm rot}\sin i < 1$ km s^{-1}. Note that atypical points which are observed at the top of the RV-A plot are certainly due to dynamical effects since they corresponds to phases of outwards acceleration.

4.3. Discussion

As observed in the particular case of ℓ Car and RS Pup, an important systematic shift in asymmetry can be present between observations and models. We define respectively $\gamma_{\rm O}$ and $\gamma_{\rm C}$ the averaged value of the observational and computed asymmetry curves [in %]. Note that the phases are sampled in the same way for data and model. Results are indicated in Table 2. We have also calculated for each star the residuals between the observational and computed asymmetry curves, noted O−C curves (Fig. 13). We define $\gamma_{\rm O-C}$, the average value of these residual curves. These O−C asymmetry curves contain the whole dynamical information present in the observational asymmetry, mainly: the limb-darkening variation in the spectral line and with the pulsation phase, the micro- and macro- turbulence, velocity gradient and temperature effects. For R TrA, S Cru, Y Sgr, RZ Vel and RS Pup, we note a bump in the O−C asymmetry curves which is approximately linked to the cross of the compression wave just after the maximum contraction velocity (see Fig. 3). However β Dor, ζ Gem and ℓ Car do not present such bump, which may be interpreted as the presence of a very small compression wave. In the case of Y Oph the phase sampling seems insufficient to conclude. Consistent hydrodynamical model would be helpful to confirm these results.

$\gamma_{\rm O}$, $\gamma_{\rm C}$ and $\gamma_{\rm O-C}$ are represented as a function of the pulsation period in Fig. 14a. The open squares represent $\gamma_{\rm C}$. We want to emphasize here that our model produces asymmetry curves with *non*-zero average value. Indeed, it is a natural consequence of the shape of the observational radial velocity curve used to derive the pulsation velocity. We find a similar behavior for all stars independently of the period.

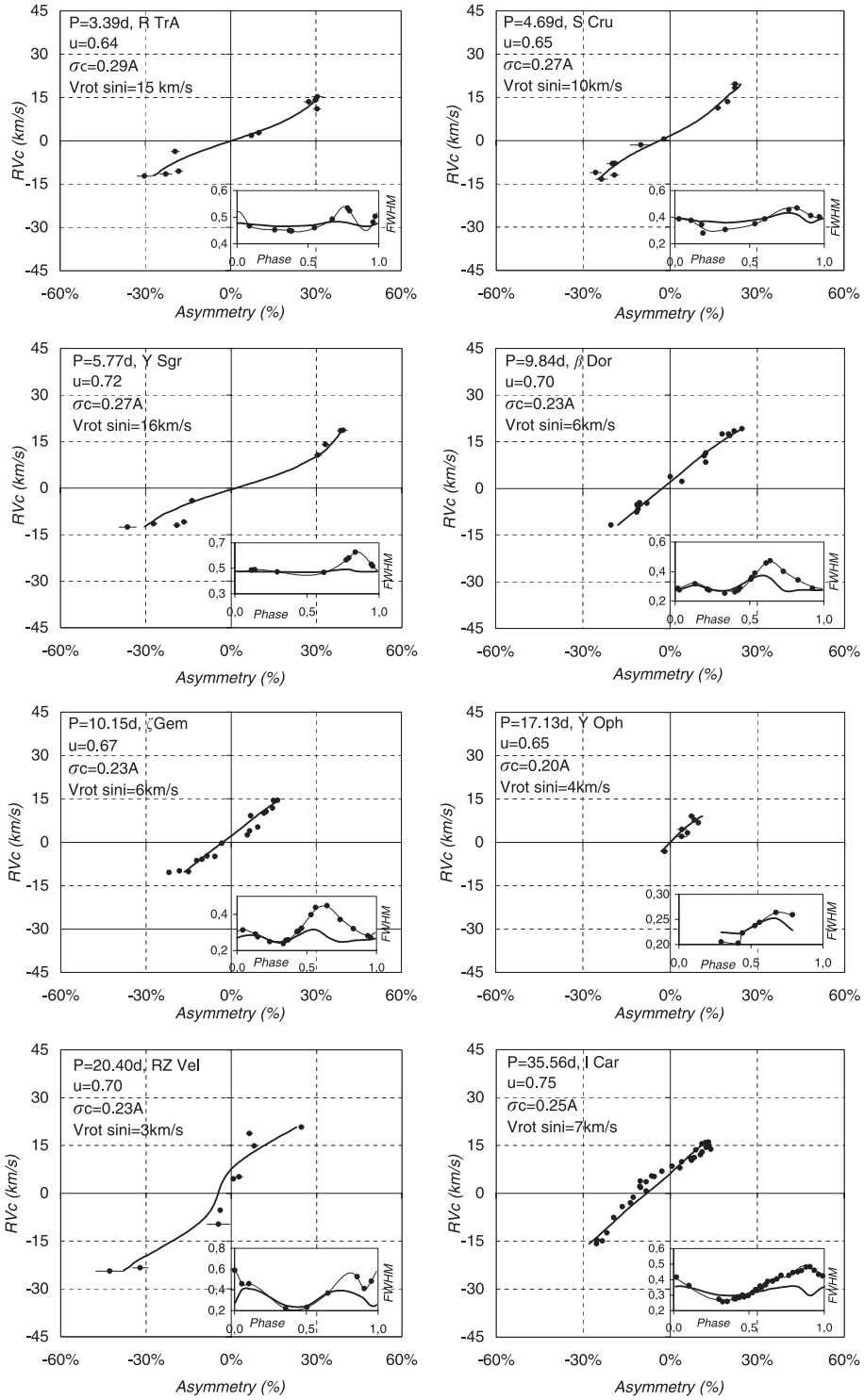

Fig. 11. Radial velocity (RV_c) – asymmetry correlation curves for R TrA, S Cru, Y Sgr, β Dor, ζ Gem, Y Oph, RZ Vel and ℓ Car. Dots and bold curves correspond respectively to observations and models. The statistical uncertainties are indicated. Note that RV-A plot deduced from the model have been shifted in asymmetry. The small plot on each diagram correspond to the comparison of the observational (dots) and model (bold curve) $FWHM$.

The shifts obtained on the observational asymmetry curves (γ_O) show a very interesting linear dependence with the logarithm of the pulsation period:

$$\gamma_O = (-10.7 \pm 0.1)\log(P) + (9.7 \pm 0.2)\ [\text{in \%}]\ . \quad (7)$$

Moreover we note that the dependence of γ_{O-C} with the pulsation period is very similar to the one of γ_O. We can conclude that this behavior is related to the dynamical effects in the atmosphere, which are not taken into account in our toy model. This can be explained by the fact that long-period Cepheids have extended atmosphere and consequently strong velocity gradient (see for example the case of RS Pup mentioned above). Thus, the line forming region can be seriously perturbed leading to a systematic shift in asymmetry (Albrow & Cottrell 1994). However,

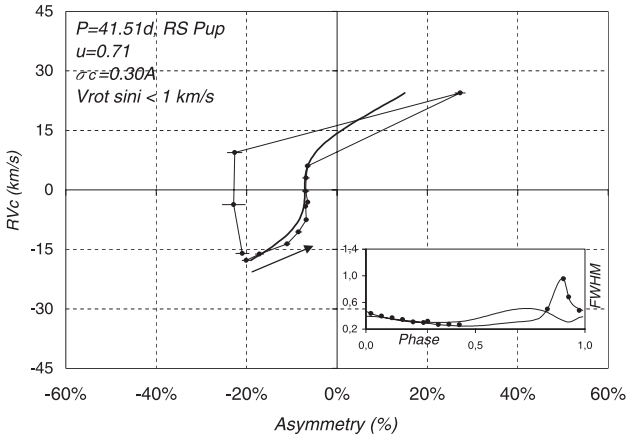

Fig. 12. Same as Fig. 11 but for RS Pup. RS Pup seems to be a non-rotating star as requested by the shape of its RV-A curve. Note also atypical points in observational RV-A plot, which can certainly be interpreted through the presence of a strong compression or shock wave in the stellar atmosphere.

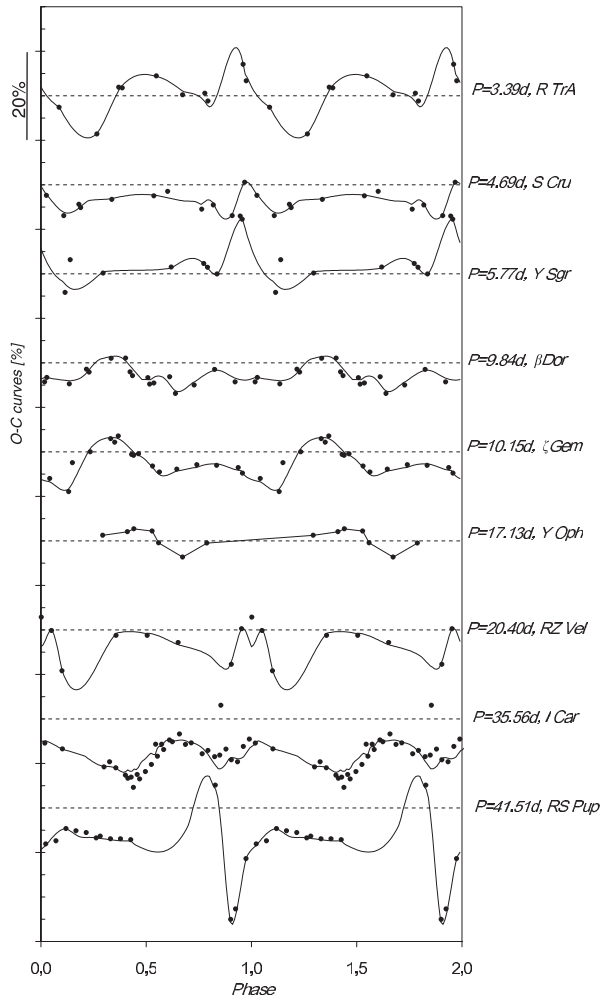

Fig. 13. Difference of the Observational and Computed asymmetry curves (O−C curves) for each stars. Curves are arbitrarily shifted. The horizontal dotted lines corresponds to a zero asymmetry for each star.

such an interpretation remains tricky and needs confirmation. Forthcoming hydrodynamical models are likely to bring out important insight in this field.

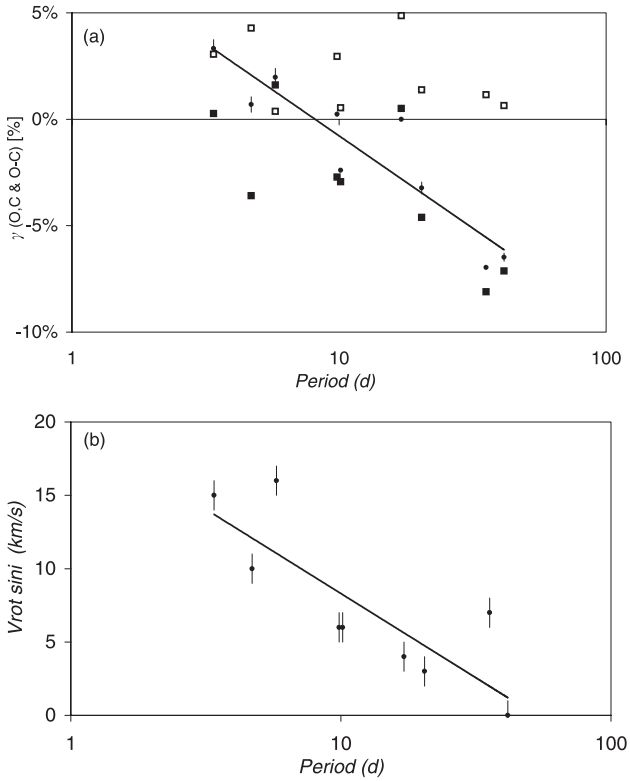

Fig. 14. a) Average values of the observational (black circles) and computed (open squares) asymmetry curves, together with the $\gamma_{\rm O-C}$ (filled squares) average values as a function of the pulsation period. **b)** Dependence of the projected rotation velocity with the pulsation period.

From results of Table 2, it appears also that the projected rotational velocity varies as a function of the pulsation period (Fig. 14b). We obtain the following relationship:

$$V_{\rm rot} \sin i = (-11.5 \pm 0.9) \log(P) + (19.8 \pm 1.0) \; [\text{in km s}^{-1}]. \quad (8)$$

The projected rotation is an important parameter which can be used, for example, to study evolution of Cepheids together with their mass loss. However, note again that our toy model does not include the physics of the pulsations and it is also very difficult to separate the rotation and macroturbulence effects in the resulting broadening of the spectral line. Thus this relation has to be considered very carefully as it is certainly model dependent.

5. Conclusion

We have presented HARPS high spectral resolution (R = 120 000) observations of nine galactic Cepheids having a good period sampling (P = 3.39d to P = 41.52d). We fit spectral line profile with an asymmetric bi-Gaussian to derive radial velocity, *FWHM* and line asymmetry for all stars. The presence of a very important compression or shock wave in the case of RS Pup, the longest period Cepheid of our sample has been identified. We have also translated the measured spectroscopic quantities into meaningful correlation curves between radial velocity and asymmetry.

A simple geometric model providing synthetic spectral lines, including limb-darkening, the $\sigma_{\rm C}$ and the projected rotation velocity is then used to interpret these correlations curves.

Firstly, we find that the centroid projection factor ($p_{\rm c}$) is independent of $\sigma_{\rm C}$ and the rotation velocity. This projection factor

is thus certainly the best one to use in the context of the Baade-Wesselink method.

Secondly, we find for each stars an optimized set of parameters which allows to reproduce observational radial velocity – asymmetry correlation curves. In particular, we find a dependence of the derived projected rotation velocities with the period of the star: $V_{\rm rot} \sin i = (-11.5 \pm 0.9) \log(P) + (19.8 \pm 1.0)$ [in km s^{-1}].

Finally, by comparing the outputs of our static models and the observed quantities, we gain access to dynamical effects. In particular, we found that long-period Cepheids with strong velocity gradient, like RS Pup, have a systematic shift in their asymmetry curve. We thus derived a linear relation between the observational shift in asymmetry and the logarithm of the period: $\gamma_{\rm O} = (-10.7 \pm 0.1) \log(P) + (9.7 \pm 0.2)$ [in %]. A detailed interpretation of these empirical relation is very difficult, but forthcoming hydrodynamical models are likely to bring out important insight in this field.

In conclusion, line asymmetry, which contains most of the physics involved in Cepheid atmosphere, is an important tool. But additional hydrodynamical considerations together with a multi-lines study are now required to have a better understanding of the dynamical processes present in Cepheid atmosphere and in particular to determine realistic projection factors including velocity gradients.

Acknowledgements. Based on observations collected at La Silla observatory, Chile, in the framework of European Southern Observatory's programs 072.D-0419 and 073.D-0136. This research has made use of the SIMBAD and VIZIER databases at CDS, Strasbourg (France). We thank David Chapeau for his helpful collaboration concerning computing aspects, Olivier Chesneau and Philippe Stee for their careful reading of the manuscript, as well as Vincent Coudé du Foresto and Andrei Fokin for useful discussions.

References

Albrow, M. D., & Cottrell, P. L. 1994, MNRAS, 267, 548
Berdnikov, L. N., & Caldwell, J. A. R. 2001, ApJ, 7, 3
Berdnikov, L. N., Dambis, A. K., & Vozyakova, O. V. 2000, A&AS, 143, 211
Bersier, D., & Burki, G. 1996, A&A, 306, 417
Burki, G., Mayor, M., & Benz, W. 1982, A&A, 109, 258
Cayrel de Strobel, G., Soubiran, C., Friel, E. D., et al. 1997, A&A, 124, 299
Cayrel de Strobel, G., Soubiran, C., & Ralite, N. 2001, A&A, 373, 159
Claret, A. 2000, A&A, 363, 1081
Fokin, A., Mathias, Ph., Chapellier, E., et al. 2004, A&A, 426, 687
Gieren, W. P., Fouqué, P., & Gómez, M. 1998, ApJ, 496, 17
Kervella, P., Nardetto, N., Bersier, D., et al. 2004, A&A, 416, 941
Kurucz, R. L. 1992, The Stellar Populations of Galaxies, IAU Symp., 149, 225
Marengo, M., Sasselov, D. D., Karovska, M., et al. 2002, ApJ, 567, 1131
Marengo, M., Karovska, M., Sasselov, D. D., et al. 2003, ApJ, 589, 975
Marengo, M., Karovska, M., Sasselov, D. D., et al. 2004, ApJ, 603, 285
Mérand, A., Kervella, P., Coude du Foresto, V., et al. 2005, A&A, 438, L9
Nardetto, N., Fokin, A., Mourard, D., et al. 2004, A&A, 428, 131
Nardetto, N., Fokin, A., Mourard, D., et al. 2006, A&A, accepted
Sabbey, C. N., Sasselov, D. D., Fieldus, M. S., et al. 1995, ApJ, 446, 250
Sasselov, D. D., & Karovska, M. 1994, ApJ, 432, 367
Sasselov, D. D., Lester, J. B., & Fieldus, M. S. 1989, ApJ, 337, 29
Sasselov, D. D., Lester, J. B., & Fieldus, M. S. 1990, ApJ, 362, 333
Szabados, L. 1989, Communications of the Konkoly Observatory Hungary, 94, 1

Online Material

Table 3. HARPS observations results for R TrA, S Cru and Y Sgr.

JD_c (a)	phase (b)	Cy. (c)	Sp. (d)	RV_g (e)	RV_m (f)	RV_c (g)	$FWHM$ (h)	D (i)	A (j)	SNR (k)	χ^2_{red} (l)
R TrA											
202.53	0.09	14	1	–26.74 ± 0.07	–29.88 ± 0.17	–25.43 ± 1.16	0.467 ± 0.009	0.14	–30.3 ± 2.7	231	2.0
206.53	0.27	15	1	–17.70 ± 0.05	–19.71 ± 0.13	–16.92 ± 0.91	0.452 ± 0.005	0.17	–19.5 ± 1.5	224	1.6
152.65	0.37	1	2	–11.18 ± 0.03	–10.41 ± 0.08	–11.39 ± 0.56	0.449 ± 0.002	0.19	7.4 ± 0.8	241	1.6
203.55	0.39	14	1	–10.08 ± 0.04	–9.06 ± 0.11	–10.47 ± 0.71	0.447 ± 0.003	0.18	9.9 ± 1.1	257	1.1
156.65	0.55	2	2	–0.98 ± 0.04	2.20 ± 0.09	–2.15 ± 0.52	0.460 ± 0.005	0.19	30.4 ± 1.3	209	1.0
204.52	0.67	14	1	3.29 ± 0.06	6.70 ± 0.15	2.02 ± 0.74	0.492 ± 0.008	0.17	30.6 ± 2.0	207	1.4
150.65	0.78	1	2	2.26 ± 0.04	5.89 ± 0.09	0.89 ± 0.50	0.534 ± 0.005	0.16	29.9 ± 1.1	255	1.3
201.54	0.79	14	1	1.34 ± 0.06	4.64 ± 0.14	0.30 ± 0.74	0.524 ± 0.007	0.16	27.5 ± 1.6	247	1.7
154.65	0.96	2	2	–24.46 ± 0.05	–26.46 ± 0.13	–23.76 ± 0.79	0.481 ± 0.004	0.12	–18.3 ± 1.4	241	1.2
205.54	0.98	15	1	–25.60 ± 0.08	–28.18 ± 0.19	–24.71 ± 1.24	0.503 ± 0.007	0.12	–22.8 ± 2.1	243	1.4
S Cru											
207.46	0.03	3	1	–21.58 ± 0.05	–23.61 ± 0.13	–20.47 ± 1.01	0.386 ± 0.005	0.16	–23.6 ± 2.0	230	1.5
151.56	0.11	1	1	–19.32 ± 0.05	–21.43 ± 0.12	–18.20 ± 0.93	0.375 ± 0.005	0.18	–25.6 ± 2.0	214	1.4
203.49	0.18	3	2	–15.82 ± 0.03	–17.26 ± 0.07	–14.98 ± 0.50	0.344 ± 0.002	0.21	–19.0 ± 1.0	224	1.7
156.63	0.19	1	1	–15.65 ± 0.04	–16.90 ± 0.10	–15.07 ± 0.52	0.281 ± 0.004	0.19	–19.8 ± 1.9	221	2.4
152.63	0.34	1	1	–6.94 ± 0.02	–7.08 ± 0.06	–6.54 ± 0.46	0.306 ± 0.001	0.26	–2.1 ± 0.8	255	1.9
153.57	0.54	1	1	4.61 ± 0.03	5.87 ± 0.08	4.21 ± 0.62	0.351 ± 0.002	0.26	16.5 ± 1.1	209	2.5
205.47	0.60	3	1	7.09 ± 0.03	8.77 ± 0.06	6.44 ± 0.59	0.386 ± 0.002	0.26	19.9 ± 0.9	269	2.5
154.64	0.76	1	1	13.40 ± 0.05	15.66 ± 0.12	12.48 ± 1.06	0.454 ± 0.005	0.23	22.5 ± 1.4	181	1.6
206.48	0.82	3	1	12.07 ± 0.04	14.42 ± 0.09	11.17 ± 0.59	0.469 ± 0.004	0.20	22.4 ± 1.0	285	1.5
150.63	0.91	1	1	–9.32 ± 0.14	–10.19 ± 0.35	–8.58 ± 1.37	0.412 ± 0.008	0.17	–10.1 ± 3.7	87	1.4
202.49	0.97	3	1	–19.91 ± 0.05	–21.62 ± 0.12	–19.05 ± 0.70	0.401 ± 0.004	0.15	–19.2 ± 1.5	287	2.0
Y Sgr											
204.63	0.12	10	2	–16.53 ± 0.06	–20.47 ± 0.15	–15.07 ± 0.86	0.485 ± 0.011	0.15	–36.4 ± 3.0	160	1.1
152.80	0.14	1	2	–15.07 ± 0.04	–18.08 ± 0.09	–14.02 ± 0.56	0.488 ± 0.004	0.16	–27.2 ± 1.3	251	1.4
205.67	0.30	10	1	–6.93 ± 0.05	–8.45 ± 0.12	–6.56 ± 0.65	0.472 ± 0.003	0.19	–13.7 ± 1.1	244	2.6
149.80	0.62	1	2	9.37 ± 0.04	12.58 ± 0.09	8.13 ± 0.62	0.467 ± 0.005	0.21	30.5 ± 1.3	178	1.0
202.65	0.77	10	2	18.50 ± 0.04	23.46 ± 0.09	16.08 ± 0.71	0.565 ± 0.007	0.19	39.5 ± 1.4	231	1.5
150.79	0.79	1	2	18.31 ± 0.03	23.31 ± 0.08	15.98 ± 0.61	0.581 ± 0.006	0.18	38.5 ± 1.1	270	1.8
156.83	0.84	2	2	13.31 ± 0.04	18.07 ± 0.11	11.56 ± 0.63	0.626 ± 0.007	0.16	33.2 ± 1.2	255	1.6
203.65	0.95	10	2	–14.27 ± 0.04	–16.27 ± 0.11	–13.47 ± 0.50	0.530 ± 0.003	0.13	–16.5 ± 1.0	288	1.4
151.75	0.96	1	2	–15.22 ± 0.05	–17.50 ± 0.12	–14.51 ± 0.61	0.517 ± 0.004	0.13	–19.1 ± 1.2	254	1.1

(a) JD_c, average Julian date of observation defined by $JD_c = JD - 2\,453\,000$ [in days].
(b) phase, averaged pulsation phase of observation. For ephemeris see Table 1.
(c) Cy., pulsating cycle of the star corresponding to observation.
(d) Sp., number of spectra associated to observation. Results corresponding to these spectra are averaged.
(e) RV_g, Gaussian fit radial velocity and the associated error barre [in km s^{-1}].
(f) RV_m, minimum radial velocity derived from the bi-Gaussian fit [in km s^{-1}].
(g) RV_c, radial velocity corresponding to the first moment of the spectral line [in km s^{-1}].
(h) $FWHM$, Full-Width at Half-Maximum derived from the bi-Gaussian fit [in Angstroms].
(i) D, line depth derived from the bi-Gaussian fit [no dimension]. Errors bars are not indicated but of the order of 10^{-4}.
(j) A, asymmetry derived from the bi-Gaussian fit [in percentage].
(k) SNR, observational spectral line signal to noise ratio.
(l) χ^2_{red}, reduced χ^2 factor corresponding to the bi-Gaussian fit.

Table 4. HARPS observations results for β Dor, ζ Gem, Y Oph, and RZ Vel. See Table3 for legend.

JD_c (a)	phase (b)	Cy. (c)	Sp. (d)	RV_g (e)	RV_m (f)	RV_c (g)	$FWHM$ (h)	D (i)	A (j)	SNR (k)	χ^2_{red} (l)
						β Dor					
21.68	0.02	1	4	1.70 ± 0.01	0.99 ± 0.02	2.17 ± 0.14	0.286 ± 0.001	0.23	–11.3 ± 0.4	345	3.7
31.64	0.03	2	3	1.35 ± 0.01	0.68 ± 0.02	1.64 ± 0.12	0.275 ± 0.001	0.23	–11.0 ± 0.4	404	2.4
32.68	0.14	2	3	–5.16 ± 0.01	–6.59 ± 0.03	–4.33 ± 0.19	0.318 ± 0.001	0.24	–20.3 ± 0.6	298	2.1
23.64	0.22	1	4	–0.73 ± 0.01	–1.42 ± 0.01	–0.19 ± 0.11	0.280 ± 0.001	0.30	–11.4 ± 0.2	423	4.9
33.61	0.23	2	3	0.15 ± 0.01	–0.49 ± 0.02	0.71 ± 0.12	0.275 ± 0.001	0.31	–11.0 ± 0.3	443	7.9
34.64	0.33	2	2	9.67 ± 0.01	9.90 ± 0.02	9.68 ± 0.22	0.253 ± 0.001	0.36	4.1 ± 0.3	330	2.5
15.62	0.40	1	3	16.16 ± 0.01	16.85 ± 0.02	15.85 ± 0.28	0.261 ± 0.001	0.35	12.3 ± 0.4	262	2.4
25.68	0.42	2	3	18.10 ± 0.01	18.80 ± 0.02	17.86 ± 0.24	0.273 ± 0.001	0.33	11.8 ± 0.3	399	3.3
35.64	0.44	3	2	19.09 ± 0.01	19.87 ± 0.02	18.80 ± 0.35	0.290 ± 0.001	0.33	12.3 ± 0.4	337	2.0
16.67	0.51	1	3	24.95 ± 0.01	26.53 ± 0.02	24.41 ± 0.38	0.347 ± 0.001	0.28	20.5 ± 0.4	352	3.2
26.59	0.52	2	2	25.48 ± 0.01	27.09 ± 0.02	24.91 ± 0.34	0.359 ± 0.001	0.27	20.2 ± 0.3	473	4.9
36.64	0.54	3	2	26.61 ± 0.01	28.52 ± 0.04	25.83 ± 0.54	0.388 ± 0.001	0.26	22.1 ± 0.5	336	2.2
17.69	0.61	1	3	27.57 ± 0.02	30.11 ± 0.04	26.60 ± 0.51	0.457 ± 0.002	0.22	24.8 ± 0.5	303	2.2
37.64	0.64	3	2	25.54 ± 0.02	27.46 ± 0.04	24.86 ± 0.45	0.473 ± 0.001	0.20	18.0 ± 0.5	409	3.1
28.67	0.73	2	3	11.09 ± 0.01	11.09 ± 0.03	11.15 ± 0.20	0.401 ± 0.001	0.21	0.1 ± 0.3	456	2.7
29.63	0.83	2	4	2.24 ± 0.01	1.65 ± 0.02	2.60 ± 0.12	0.343 ± 0.001	0.23	–7.9 ± 0.2	472	6.5
30.59	0.92	2	3	2.36 ± 0.01	1.71 ± 0.02	2.77 ± 0.12	0.286 ± 0.001	0.24	–10.5 ± 0.3	455	5.0
						ζ Gem					
32.70	0.04	2	3	–3.82 ± 0.02	–5.04 ± 0.04	–3.05 ± 0.33	0.313 ± 0.001	0.27	–18.2 ± 0.7	196	2.9
33.62	0.14	2	3	–4.67 ± 0.01	–6.02 ± 0.02	–3.55 ± 0.19	0.292 ± 0.001	0.31	–21.9 ± 0.4	330	7.7
23.65	0.15	1	4	–4.00 ± 0.01	–4.89 ± 0.02	–3.35 ± 0.13	0.276 ± 0.001	0.31	–15.0 ± 0.3	338	4.2
34.65	0.23	2	3	1.53 ± 0.01	1.23 ± 0.02	1.97 ± 0.15	0.248 ± 0.001	0.37	–5.7 ± 0.3	334	6.0
35.65	0.34	2	3	9.44 ± 0.01	9.73 ± 0.02	9.41 ± 0.18	0.239 ± 0.001	0.39	5.8 ± 0.3	299	2.6
25.69	0.35	1	3	10.86 ± 0.01	11.22 ± 0.03	10.84 ± 0.35	0.256 ± 0.001	0.37	6.6 ± 0.4	195	1.9
15.71	0.37	1	3	12.29 ± 0.01	12.81 ± 0.02	12.12 ± 0.25	0.259 ± 0.001	0.38	9.4 ± 0.3	253	1.6
36.66	0.43	2	2	17.10 ± 0.01	17.87 ± 0.03	16.92 ± 0.46	0.304 ± 0.001	0.34	11.7 ± 0.5	255	2.3
26.60	0.44	2	3	17.69 ± 0.01	18.53 ± 0.02	17.48 ± 0.29	0.308 ± 0.001	0.33	12.4 ± 0.3	353	3.1
16.69	0.46	1	3	19.06 ± 0.02	20.11 ± 0.04	18.71 ± 0.50	0.324 ± 0.001	0.31	14.6 ± 0.6	189	1.4
37.66	0.53	3	2	21.81 ± 0.01	23.27 ± 0.03	21.40 ± 0.45	0.397 ± 0.001	0.28	16.4 ± 0.4	341	3.1
17.70	0.56	1	3	21.79 ± 0.01	23.25 ± 0.02	21.35 ± 0.33	0.439 ± 0.001	0.27	14.9 ± 0.2	446	3.1
28.68	0.62	2	2	16.11 ± 0.02	16.81 ± 0.06	16.02 ± 0.59	0.449 ± 0.001	0.24	7.0 ± 0.6	243	1.4
29.64	0.74	2	2	6.25 ± 0.03	5.98 ± 0.07	6.53 ± 0.53	0.372 ± 0.001	0.26	–3.3 ± 0.8	169	1.7
30.60	0.84	2	3	1.64 ± 0.01	1.06 ± 0.02	2.09 ± 0.16	0.321 ± 0.001	0.28	–8.5 ± 0.3	407	7.2
31.64	0.94	2	3	0.49 ± 0.01	–0.13 ± 0.02	0.98 ± 0.15	0.282 ± 0.001	0.28	–10.2 ± 0.3	372	8.3
21.70	0.96	1	5	0.18 ± 0.01	–0.54 ± 0.03	0.59 ± 0.15	0.271 ± 0.001	0.27	–12.1 ± 0.5	229	2.3
						Y Oph					
216.75	0.29	4	1	–9.75 ± 0.02	–9.83 ± 0.05	–9.72 ± 0.46	0.205 ± 0.001	0.32	–1.9 ± 1.1	189	1.2
201.63	0.41	4	1	–4.48 ± 0.03	-4.31 ± 0.08	–4.57 ± 0.43	0.202 ± 0.002	0.31	4.0 ± 1.8	119	1.4
150.78	0.44	1	1	–3.15 ± 0.02	–2.87 ± 0.04	–3.37 ± 0.27	0.223 ± 0.001	0.33	5.9 ± 0.7	262	2.9
203.65	0.53	4	1	0.57 ± 0.02	1.06 ± 0.04	0.20 ± 0.22	0.238 ± 0.001	0.31	9.7 ± 0.7	296	4.3
152.80	0.56	1	1	1.37 ± 0.02	1.80 ± 0.04	1.09 ± 0.24	0.244 ± 0.001	0.30	8.3 ± 0.7	297	3.8
154.75	0.67	1	1	2.89 ± 0.03	3.30 ± 0.07	2.47 ± 0.41	0.263 ± 0.001	0.27	7.4 ± 1.1	208	3.6
156.71	0.79	1	1	–1.85 ± 0.04	–1.62 ± 0.10	–2.13 ± 0.63	0.259 ± 0.002	0.26	4.1 ± 1.6	142	2.5
						RZ Vel					
204.44	0.00	3	1	13.05 ± 0.23	12.50 ± 0.58	14.39 ± 4.04	0.588 ± 0.012	0.14	–4.4 ± 4.0	76	1.3
205.44	0.05	3	1	–0.47 ± 0.07	–3.76 ± 0.16	0.69 ± 0.78	0.457 ± 0.009	0.16	–32.0 ± 2.7	210	1.5
206.44	0.10	3	1	–1.90 ± 0.08	–6.21 ± 0.17	–0.30 ± 0.96	0.459 ± 0.016	0.17	–42.7 ± 4.9	162	2.5
150.49	0.36	1	1	18.65 ± 0.01	18.46 ± 0.03	18.76 ± 0.38	0.219 ± 0.001	0.38	–3.9 ± 0.5	309	7.8
152.51	0.46	1	1	28.82 ± 0.01	28.83 ± 0.02	28.61 ± 0.60	0.231 ± 0.001	0.41	0.8 ± 0.5	205	2.8
154.50	0.55	1	1	45.64 ± 0.02	47.66 ± 0.05	44.86 ± 1.46	0.369 ± 0.002	0.32	24.7 ± 0.9	239	3.2
156.49	0.65	1	1	43.14 ± 0.05	43.91 ± 0.14	42.87 ± 2.31	0.526 ± 0.003	0.23	6.4 ± 1.1	178	1.8
201.44	0.86	3	1	39.12 ± 0.04	39.87 ± 0.09	38.93 ± 1.45	0.411 ± 0.002	0.24	8.1 ± 1.0	224	2.7
202.45	0.90	3	1	29.54 ± 0.06	29.84 ± 0.15	29.26 ± 1.09	0.483 ± 0.003	0.14	2.8 ± 1.2	271	1.2
203.44	0.95	3	1	13.05 ± 0.23	12.50 ± 0.58	14.39 ± 4.04	0.588 ± 0.012	0.14	–4.4 ± 4.0	76	1.3

Table 5. HARPS observations results for ℓ Car and RS Pup. See Table 3 for legend.

JD_c (a)	phase (b)	Cy. (c)	Sp. (d)	RV_g (e)	RV_m (f)	RV_c (g)	*FWHM* (h)	*D* (i)	*A* (j)	*SNR* (k)	χ^2_{red} (l)
						ℓ Car					
37.65	0.02	1	7	–13.40 ± 0.01	–15.70 ± 0.02	–12.19 ± 0.18	0.416 ± 0.001	0.26	–25.4 ± 0.3	354	3.5
40.63	0.10	1	5	–12.24 ± 0.01	–14.22 ± 0.02	–11.10 ± 0.17	0.362 ± 0.001	0.31	–25.2 ± 0.3	333	3.6
47.69	0.30	1	2	–1.57 ± 0.01	–2.51 ± 0.02	–0.61 ± 0.24	0.274 ± 0.001	0.42	–16.4 ± 0.4	275	7.5
48.62	0.33	1	2	–0.01 ± 0.01	–0.76 ± 0.01	0.59 ± 0.10	0.257 ± 0.001	0.40	–13.7 ± 0.2	438	10.3
49.67	0.36	1	2	1.79 ± 0.01	1.09 ± 0.02	2.34 ± 0.13	0.260 ± 0.001	0.40	–12.7 ± 0.3	374	6.0
15.72	0.40	1	3	4.92 ± 0.00	4.33 ± 0.01	5.42 ± 0.12	0.276 ± 0.001	0.40	–10.2 ± 0.2	405	7.0
51.68	0.41	2	4	5.23 ± 0.00	4.62 ± 0.01	5.75 ± 0.13	0.274 ± 0.001	0.39	–10.4 ± 0.2	352	6.0
16.69	0.43	1	3	6.64 ± 0.01	6.13 ± 0.02	7.15 ± 0.21	0.289 ± 0.001	0.39	–8.3 ± 0.3	293	5.6
52.64	0.44	2	2	6.93 ± 0.01	6.30 ± 0.02	7.42 ± 0.18	0.285 ± 0.001	0.39	–10.3 ± 0.3	376	5.4
17.71	0.46	1	3	8.46 ± 0.01	8.11 ± 0.01	8.86 ± 0.15	0.300 ± 0.001	0.38	–5.5 ± 0.2	444	8.7
53.69	0.47	2	2	8.70 ± 0.01	8.31 ± 0.02	9.00 ± 0.18	0.288 ± 0.001	0.37	–6.3 ± 0.3	390	5.0
54.67	0.50	2	2	10.36 ± 0.01	10.18 ± 0.02	10.52 ± 0.22	0.296 ± 0.001	0.35	–2.9 ± 0.3	340	4.7
55.70	0.53	2	2	11.99 ± 0.01	12.04 ± 0.02	12.08 ± 0.20	0.316 ± 0.001	0.35	0.6 ± 0.2	418	4.5
20.84	0.54	1	3	14.11 ± 0.01	14.65 ± 0.03	13.93 ± 0.35	0.335 ± 0.001	0.33	7.4 ± 0.4	218	2.2
56.70	0.55	2	2	13.46 ± 0.01	13.75 ± 0.02	13.42 ± 0.25	0.331 ± 0.001	0.34	4.0 ± 0.3	378	4.2
21.85	0.57	1	3	15.01 ± 0.01	15.66 ± 0.02	14.76 ± 0.22	0.358 ± 0.001	0.32	8.3 ± 0.2	379	3.6
57.70	0.58	2	2	14.82 ± 0.01	15.35 ± 0.02	14.67 ± 0.27	0.347 ± 0.001	0.34	7.0 ± 0.3	384	3.7
58.71	0.61	2	2	16.00 ± 0.01	16.83 ± 0.02	15.70 ± 0.27	0.365 ± 0.001	0.33	10.5 ± 0.3	412	5.3
23.66	0.62	1	4	16.98 ± 0.01	17.92 ± 0.02	16.55 ± 0.20	0.388 ± 0.001	0.31	11.1 ± 0.2	428	3.5
24.85	0.66	1	4	17.94 ± 0.01	19.15 ± 0.02	17.43 ± 0.22	0.389 ± 0.001	0.30	14.0 ± 0.2	374	3.6
25.87	0.69	1	4	18.52 ± 0.01	19.63 ± 0.02	18.00 ± 0.19	0.404 ± 0.001	0.30	12.4 ± 0.2	492	4.2
26.85	0.71	1	5	19.03 ± 0.01	20.27 ± 0.02	18.50 ± 0.24	0.426 ± 0.001	0.31	13.4 ± 0.2	436	5.9
28.69	0.77	1	5	20.12 ± 0.01	21.26 ± 0.02	19.50 ± 0.22	0.426 ± 0.001	0.29	12.2 ± 0.2	433	3.1
29.65	0.79	1	5	20.33 ± 0.01	21.61 ± 0.02	19.63 ± 0.23	0.445 ± 0.001	0.29	13.2 ± 0.2	439	4.7
30.80	0.83	1	7	19.76 ± 0.01	20.83 ± 0.01	19.05 ± 0.19	0.450 ± 0.001	0.28	11.0 ± 0.1	446	6.6
31.66	0.85	1	5	17.77 ± 0.01	18.65 ± 0.02	17.15 ± 0.24	0.458 ± 0.001	0.27	8.9 ± 0.2	391	5.3
32.72	0.88	1	5	11.81 ± 0.01	12.17 ± 0.02	11.51 ± 0.20	0.481 ± 0.001	0.24	3.4 ± 0.2	431	3.8
33.63	0.91	1	5	3.92 ± 0.01	3.06 ± 0.03	4.31 ± 0.20	0.483 ± 0.001	0.23	–8.2 ± 0.2	371	4.1
34.67	0.93	1	5	–4.93 ± 0.01	–6.89 ± 0.02	–3.99 ± 0.15	0.460 ± 0.001	0.24	–19.5 ± 0.2	486	8.3
35.66	0.96	1	7	–9.85 ± 0.01	–11.93 ± 0.02	–8.81 ± 0.14	0.434 ± 0.001	0.24	–21.8 ± 0.2	421	6.0
36.65	0.99	1	6	–12.39 ± 0.01	–14.56 ± 0.02	–11.29 ± 0.21	0.423 ± 0.001	0.24	–23.4 ± 0.3	327	2.8
						RS Pup					
56.68	0.02	1	1	3.58 ± 0.03	1.58 ± 0.07	4.33 ± 0.41	0.433 ± 0.003	0.20	–20.1 ± 0.9	347	2.1
58.69	0.07	1	1	5.31 ± 0.03	3.78 ± 0.07	5.94 ± 0.46	0.395 ± 0.002	0.23	–17.1 ± 0.9	277	2.0
60.68	0.12	1	1	7.95 ± 0.02	6.97 ± 0.05	8.50 ± 0.42	0.370 ± 0.001	0.26	–11.0 ± 0.7	315	2.3
62.67	0.17	1	1	10.99 ± 0.02	10.28 ± 0.05	11.48 ± 0.55	0.343 ± 0.001	0.29	–8.5 ± 0.7	258	2.8
64.68	0.22	1	1	14.21 ± 0.01	13.70 ± 0.04	14.55 ± 0.41	0.307 ± 0.001	0.32	–6.8 ± 0.5	328	3.2
66.66	0.26	1	1	17.46 ± 0.01	16.96 ± 0.03	17.96 ± 0.58	0.296 ± 0.001	0.36	–6.9 ± 0.5	308	3.8
150.48	0.28	3	1	18.43 ± 0.01	17.89 ± 0.03	18.96 ± 0.64	0.317 ± 0.001	0.37	–6.5 ± 0.5	310	2.9
152.49	0.33	3	1	21.56 ± 0.02	21.15 ± 0.04	21.79 ± 0.59	0.269 ± 0.001	0.34	–6.9 ± 0.7	249	7.2
154.49	0.38	3	1	24.80 ± 0.02	24.38 ± 0.05	25.12 ± 0.89	0.271 ± 0.001	0.36	–6.9 ± 0.7	211	3.0
156.48	0.43	3	2	27.90 ± 0.01	27.52 ± 0.04	28.12 ± 0.67	0.264 ± 0.001	0.34	–6.5 ± 0.6	202	4.1
48.61	0.83	1	1	47.56 ± 0.04	50.66 ± 0.09	46.52 ± 1.69	0.499 ± 0.004	0.24	27.3 ± 1.1	239	3.3
51.64	0.90	1	1	30.44 ± 0.11	25.29 ± 0.27	31.52 ± 2.02	0.955 ± 0.010	0.12	–22.6 ± 1.6	249	2.6
52.63	0.93	1	1	16.40 ± 0.12	12.85 ± 0.30	18.39 ± 1.97	0.681 ± 0.012	0.13	–22.8 ± 2.5	173	1.3
54.66	0.97	1	1	5.26 ± 0.05	2.97 ± 0.13	6.07 ± 0.71	0.479 ± 0.005	0.17	–20.9 ± 1.5	247	1.0